Journal of Solar Energy Research (JSER)

Journal homepage: jser.ut.ac.ir

AUTOREGRESSIVE NEURAL NETWORK MODELS FOR SOLAR POWER FORECASTING OVER NIGERIA

Omitusa Oluwafemi Olatunde*, Ojo Olusola Samuel, Emmanuel Israel and Adeyemi Babatunde

Department of Physics, Federal University of Technology Akure, P.M.B. 704, Akure, Ondo State, Nigeria
Received: 2021-06-18
Accepted: 2021-09-06

Abstract

In this study, the nonlinear autoregressive neural network with exogenous input (NARX) model was employed to predict solar power in different geoclimatic zones of Nigeria using six solar radiation parameters. The solar power was first deduced using the surface direct and diffuse solar radiation data obtained from the archives of the Modern-Era Retrospective Analysis for Research and Application, Version 2, over 20 stations spread across Nigeria. NARX model was then created and trained using Levenberg-Marquardt (LM), Bayesian regularization (BR), scaled conjugate gradient (SCG), and Broyden–Fletcher–Goldfarb–Shanno (BFGS) algorithms, and the values were compared to the calculated values of the solar power. The performance of the four algorithms were assessed using standard evaluation metrics. Error analyses showed that all the algorithms had desirable performances with root mean square error (RMSE) values ranging from 0.162 to 0.544 W/m^2. Regionally, the NARX-BFGS model had the best performance in the Coastal and Guinea Savanna zones, whereas the NARX-LM and NARX-BR models had the best performances in the Sahel and Derived Savanna zones, respectively. The results of this study will assist solar engineers in calibrating the performance of solar conversion systems for the future planning of sustainable renewable energy policies.

Keywords: NARX, solar power, artificial neural network, renewable energy, Broyden–Fletcher–Goldfarb–Shanno

1. Introduction

Renewable energy sources are resources that can be efficiently utilized to counter energy shortfalls and ever-increasing electricity demands in Nigeria (Olusola et al., 2020). One of the viable renewable energy sources in Nigeria is the sun, as researches have shown that solar radiation is abundant in the north east, north west, and north central geo-political zones of the country (Bugaje 2006). Solar energy is mainly influenced by the incoming solar radiation, characteristics of the solar panel, and several other factors including atmospheric conditions, trajectory of the sun, tilt angle of the solar panel relative to the sun, weather conditions, cloud cover, and the physical properties of the solar energy plant that convert solar energy to electric power (Awan, Khan, and Aslam 2018). Thus, the knowledge and consideration of these factors are essential for the accurate estimation of solar energy. However, insitu solar radiation data are rarely available in Nigeria owing to the high costs associated with purchasing and maintaining the measuring equipment. Moreover, the calculation of the solar power on a tilted plane is complex; hence, most studies usually rely on assumptions which may lead to poor performance (Olusola et al., 2020).

In recent times, artificial intelligence (AI) methods have been used to learn the relationships between predicted and actual outputs using time-series historical data (Abuella and Chowdhury 2015). AI methods utilize algorithms that can implicitly describe the nonlinear and highly complex relationships between input data and output power rather than an explicit statistical analysis, thereby significantly reducing the complexity associated with prediction calculations (Abuella and Chowdhury 2015; Maind and Wankar 2014). For both statistical and AI approaches, high-quality time series data comprising weather predictions and power outputs

*Corresponding author. Email: omitusaf@gmail.com.

from the past are very important. One of the most common AI models is the artificial neural network (ANN). ANNs are particularly suited for solving problems that are difficult to model analytically, and they have been applied in several areas such as pattern recognition systems, optimization, signal processing, and prediction (Rajendra et al. 2019). The operations of ANNs are similar to those of the human brain in which knowledge is acquired through learning and stored using weights, which are the internal connections between the neurons (Ojo, Adeyemi, and Oluleye 2020; Sözen et al. 2005).

Several researchers have demonstrated the suitability of the nonlinear autoregressive network with exogenous inputs (NARX) network model for modeling nonlinear systems over classical modeling approaches and other ANNs (Inman, Pedro, and Coimbra 2013; Ojo, Adeyemi, and Oluleye 2020; Sani et al. 2014). The key advantages of the NARX network model over other neural network models are its better generalization ability, faster convergence, and ability to remember information stored for a long period of time (Haddad et al. 2015; Çoruh et al. 2014). (Haddad et al. 2015) compared different ANN models for the prediction of the water flow rate in a photovoltaic water pumping system, and they found that NARX model offered a slightly better performance than nonlinear autoregressive model and generalized regression neural network. Moreover, (Tikyaa et al. 2018) predicted solar radiation in Makurdi using a hybrid SARIMA-NARX nonlinear dynamics model. They found that the model had good accuracy after validation with an R value of 0.771. Similarly, (Ozoegwu 2019) predicted solar radiation using NARX model over six locations in Nigeria, and found that the model had the best performance in Abuja with an R value of 0.78. Furthermore, (Ojo and Adeyemi 2020) estimated the global solar radiation in Nigeria using NARX, and compared the results with those of multivariate linear regression (MLR). They discovered that the NARX model gave a better prediction of global solar radiation than the MLR model for all the zones in Nigeria. However, to the best of our knowledge, no study has reported the best NARX algorithm that is appropriate for the prediction of solar power over different geoclimatic zones of Nigeria.

In this study, the solar power was predicted from six solar radiation parameters using the NARX model with four optimization algorithms, namely Bayesian regularization (NARX-BR), Levenberg–Marquardt (NARX-LM), scaled conjugate gradient (NARX-SCG), and Broyden–Fletcher–Goldfarb–Shanno (BARX-BFGS). The best optimization algorithm that produced the highest solar power in each zone were then identified after their performance had been evaluated using standard statistical metrics such as root mean square error (RMSE), coefficient of determination (R^2), Theil's inequality coefficient (U), and standard deviation reduction (SDR). The rest of this paper is organized as follows: The methodology is presented in Section 2. The results are discussed in Section 3, and conclusions are provided in Section 4.

MATERIALS AND METHODS

The surface data of direct and diffuse solar radiation on hourly time-series format from 2013–2017 were obtained from the archives of the Modern-Era Retrospective Analysis for Research and Application, Version 2 (MERRA-2) for twenty stations spread across Nigeria, as shown in Fig. 1. The MERRA-2 data is powered by Earth Observing System Data and Information System, the key core capability in the National Aeronautics and Space Administration Earth Science Data Systems program [19]. The data gridded in NetCDF format at a spatial resolution of 0.5° x 0.63° was converted into a readable format using Ferret software.

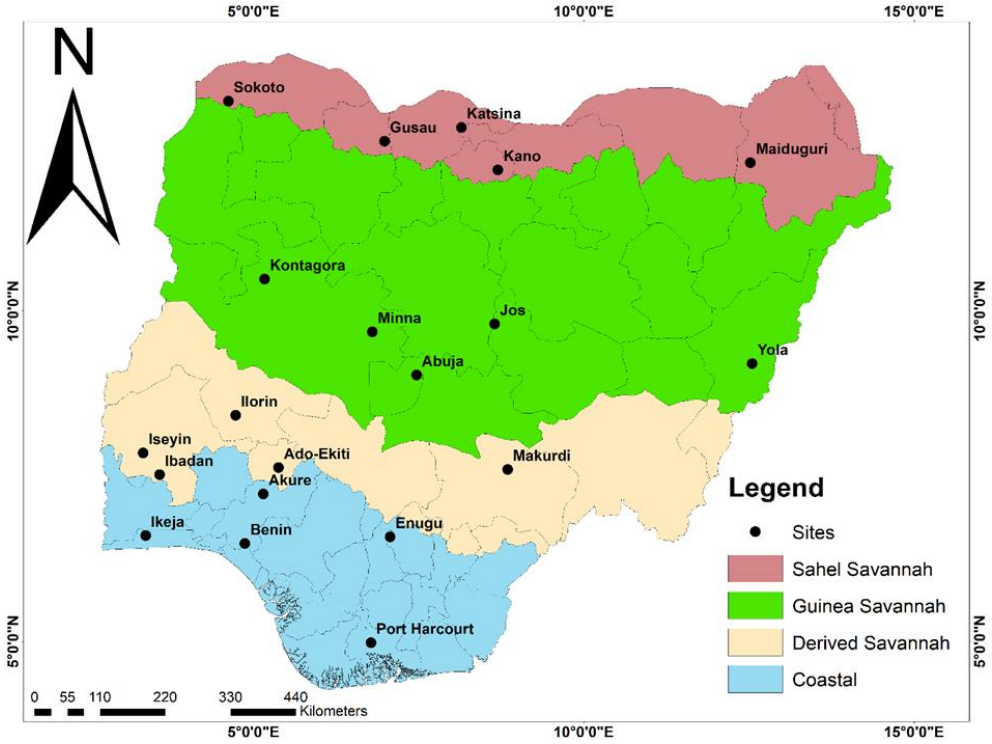

Fig. 1 Map of Nigeria showing the study locations (Olusola et al., 2020)

Data preprocessing was performed by normalizing the time series data–to have values between 0 and 1 because each dataset had different magnitudes. This process ensures that measured values with different scales are converted to a common scale. The equation for the normalization is given by Eq. (1) (Mohanty, Patra, and Sahoo 2016):

$$X_{normalized} = \frac{(X - X_{\min})}{(X_{\max} - X_{\min})} \tag{1}$$

The solar radiation parameters used as input parameters of the model were solar declination angle, sunlight duration, hour angle, solar zenith angle, solar elevation angle, and solar azimuth angle, which are briefly described below:

The solar declination angle δ is the angle between a line joining the centers of the sun and the earth (Iqbal 1983). For a particular day, δ is calculated by (Pandey and Katiyar 2009):

$$\delta = \frac{23.45\pi}{180} \sin\left[\frac{2\pi(284+n)}{365}\right] \tag{2}$$

where n is the nth day of the year.

The solar azimuth ψ is the angle at the local zenith between the plane of the observer's meridian and the plane of a great circle passing through the zenith and the sun (Iqbal 1983). It is measured east positive, west negative (south zero) and is given by:

$$\psi = \sin^{-1}\left(\frac{\cos\delta \sin\omega}{\cos\alpha}\right) \tag{3}$$

where ω is the hour angle and α is the solar elevation angle.

The hour angle ω is the angle measured at the celestial pole between the observer's meridian and the solar meridian (Iqbal 1983), and it is given by:

$$\omega = \cos^{-1}\left(-\tan\varphi \tan\delta\right) \tag{4}$$

where φ is the latitude.

The solar zenith angle θ_z (also called the zenith distance) is the angle between the local zenith and the line joining the observer (Iqbal 1983), and it is given by:

$$\theta_z = \cos^{-1}(\sin\delta\sin\varphi + \cos\delta\cos\phi\cos\omega) = \sin\omega \tag{5}$$

The solar elevation angle α (also called the solar altitude) is the sun's angular height above the observer's celestial horizon (Iqbal 1983). It is the complement of the zenith angle, and it is given by:

$$\alpha = 90 - \theta_z \tag{6}$$

The solar power E was computed using Eq. (7) for a 60-cell solar panel with an area of 1.66 m^2 and electrical power of 250 Wp according to (Markos and Sentian 2016):

$$E = A \times r \times H \times PR \tag{7}$$

where A = total solar panel area (m^2), H = monthly average global solar radiation on tilted panels, PR = performance ratio (0.75) (Markos and Sentian 2016), r is the solar panel yield (%) given by:

$$r = \frac{electric\ power\ of\ one\ solar\ panel\ (KW)}{area\ of\ one\ panel} \tag{8}$$

Meanwhile, H was computed by summing the beam, diffuse, and ground-reflected radiations as follows:

$$H_g = H_b + H_s + H_r \tag{9}$$

where H_b, H_s, and H_r are the daily beam, diffuse, and ground-reflected radiations received on an inclined surface. The calculations for the radiations are given below:

The daily beam radiation received on an inclined surface can be expressed as:

$$H_b = (H_g - H_d)R_b \tag{10}$$

where H_g and H_d are the monthly mean daily global and diffuse radiations on the horizontal surface, and R_b is the beam radiation conversion factor. According to (El-Sebaii et al. 2010), R_b can be expressed as:

$$R_b = \frac{\cos(\varphi-\beta)\cos\delta\sin\omega + \omega\sin(\varphi-\beta)\sin\delta}{\cos\varphi\cos\delta\sin\omega + \omega\sin\delta\sin\delta} \tag{11}$$

where β is the tilt angle, δ is the declination angle, and ω is the hour angle for the tilted surface.

The daily diffuse radiation was estimated using Klucher model (Pandey and Katiyar 2009), as it has a good agreement with the experimental value for all types of slope:

$$H_s = \frac{1}{2} H_d (1+\cos\beta)\left[1+F\sin^3\left(\frac{\beta}{2}\right)\right](1+F\cos^2\varphi\sin^3\varphi_z) \quad (12)$$

where H_s is the sky-diffuse radiation, H_d is the daily diffuse solar radiation on horizontal surface, β is tilt angle, φ_z is the solar zenith angle, φ is solar incidence angle on tilted plane, and F is a modulating function. The modulating function can be obtained using:

$$F = 1-\left(\frac{H_d}{H}\right)^2 \quad (13)$$

When the skies are overcast, F is zero. For clear sky conditions, F is one.

The solar incidence angle (Iqbal 1983) on tilted plane is given by:

$$\theta = \cos^{-1}[\sin\delta\sin(\varphi-\beta)+\cos\delta\cos(\varphi-\beta)\cos\omega] \quad (14)$$

The daily ground-reflected radiation was obtained using anisotropic model (Katiyar and Panday 2010), given by:

$$H_r = \sum_i^{day}\left[\frac{1}{2} I\rho(1-\cos\beta)[1+\sin^2\left(\frac{\theta_z}{2}\right)]\right](|\cos\Delta|) \quad (15)$$

where Δ is the azimuth of the tilted surface with respect to that of the sun, θ_z is the solar azimuth angle, ρ is the albedo, β is the tilt angle.

NARX is a recurrent dynamic network with feedback connections enclosing several layers of the network. It has been demonstrated to be well suited for modeling nonlinear systems, especially time series, as it is based on the linear ARX model, which is commonly used in time-series modeling (Diaconescu 2008). The main advantage of NARX over feedback neural networks is that it can accept time series represented as dynamic inputs (Ojo and Adeyemi 2020). Moreover, NARX models have a better performance in discovering long-term characteristics and behavior than traditional recurrent networks based on the back-propagation through time algorithm [31]. NARX has been extensively utilized in several applications, including pattern classification (Bishop 1995), forecasting, function approximation, optimization, and control systems [33]. The equation for the NARX model is given by (Ojo and Adeyemi 2020):

$$y(t) = f(y(t-1), y(t-2), ..., y(t-n_y, u(t-1), u(t-2, ...u(t-n_u)) \quad (16)$$

where $y(t)$ is the output signal and $u(t)$ is the input (exogenous) signal. The next value of the dependent output signal $y(t)$ is regressed on the previous values of the output signal and previous values of an independent/external (exogenous) input signal. Figure 2 shows a block diagram which represents a NARX model (Ojo and Adeyemi 2020).

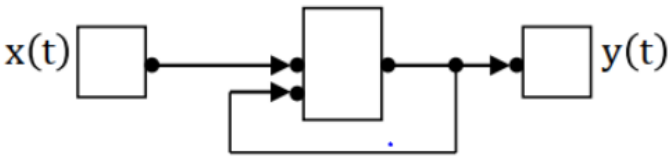

Fig. 2 NARX block diagram

The output of the NARX model is considered an approximation of the actual output of a nonlinear dynamic system because the actual output is produced during the network training phase, and a

series-parallel design is used to replace the estimated goal with the actual output (Ojo and Adeyemi 2020). NARX uses optimization algorithms to obtain the best network for time-series predictions. The optimization algorithms adopted in this study are briefly described below.

The LM algorithm is one of the most widely used functions for time series network predictions and training (Zhang and Behera 2012; Verma et al. 2016; Fentis et al. 2017). It is a variation of the Gauss–Newton algorithm that finds the function minima and optimizes the solution. It uses an approximation of the Hessian matrix as given below (Guzman, Paz, and Tagert 2017):

$$\Delta w = [J^T J + \mu I]^{-1} J^T(w) e(w) \tag{17}$$

where w is the weight, $J^T J$ represents the Hessian matrix, J is the Jacobian matrix, μ is the learning constant, J^T is the transpose of J, I is the identity matrix and e represents the vector of errors. The learning constant μ is adjusted based on the error in each iteration to find the minima. In this study, the iteration process started with a random μ for the weight optimization.

The BR backpropagation algorithm provides robust estimation for noisy and difficult inputs when sufficient amount of training data are available (Jazayeri, Jazayeri, and Uysal 2016). Regularization reduces the probability of overfitting the model by setting the optimal performance function to provide an efficient generalization based on Bayesian inference techniques (Guzman, Paz, and Tagert 2017). The algorithm works effectively by eliminating network weights that do not have a significant impact on the problem solution and it shows good performance in avoiding local minima difficulties. It does not require cross-validation; hence, some data do not need to be reserved for validation purposes. Moreover, it prevents the ANN from over-training and over-fitting problems. The objective function of the BR algorithm is given by (Kumar, Merchant, and Desai 2004):

$$F = \alpha E_w + \beta E_d, E_w = \sum_{i=1}^{N} w_i^2 \tag{18}$$

where E_w is the sum of squares of the network weights, and α and β are objective function parameters. The smaller the weights, the better the generalization capability of the network.

In numerical optimization, the BFGS algorithm is an iterative method for solving unconstrained nonlinear optimization problems (Mukherjee and Routroy 2012). The BFGS algorithm is implemented by estimating the inverse odd Hessian function H directly with a symmetric positive definite matrix P iteratively using the following steps (Asirvadam, McLoone, and Irwin 2004):

Step 1: The search direction d_k is set to be equal to $-P_{k-1} g_k$ where P_{k-1} and g_k are the approximation to inverse H_{k-1} and its gradient, respectively, at the *k*th iteration. The convergence tolerance is set to be a minimum value of order 10^{-3}.

Step 2: The weights which yield the minimum error along d_k is obtained by:

$$w_{k+1} = w_k + \eta_o d_k \tag{19}$$

$$\eta_o = \min[E(w_k + \eta d_k)] \tag{20}$$

Step 3: The new gradient g_{k+1} is computed and the approximation to P_k is updated using the new weight and gradient information given as:

$$s_k = w_{k+1} - w_k \quad \text{and} \quad y_k = g_{k+1} - g_k \tag{21}$$

$$u_k = \left(1 + \frac{y_k^T P_k y_k}{s_k^T y_k}\right)\frac{s_k^T s_k}{s_k^T y_k}, \qquad v_k = \frac{y_k^T P_k y_k + P_k y_k s_k}{s_k^T y_k} \tag{22}$$

$$P_k = P_{k+1} + u_k + v_k \tag{23}$$

The initial approximation to the inverse Hessian matrix (P_o) is an identity matrix (I) which corresponds to the steepest descent $(d_k = -g_k)$. Matrices u, v, and P are symmetric and therefore lead to a reduction of the weight errors to meet the convergence tolerance (Ojo, Adeyemi, and Oluleye 2020).

The SCG algorithm uses second order information from the neural network. However, it requires only $O(N)$ memory usage, where N is the number of weights in the network (Mishra, Prusty, and Hota 2016). Its objective function is given by:

$$E(w+y) \approx E(w) + E^{'}(w)^T y + \frac{1}{2} y^T E^{''}(w) y \tag{24}$$

where w is the weight vector, $E(w)$ is the global error function, $E^{'}(w)$ is the gradient, and $E^{''}(w)$ is the Hessian matrix.

In this study, the method proposed by (Rajendra et al. 2019; Ojo, Adeyemi, and Oluleye 2020) was used to obtain the optimal number of hidden nodes necessary for generating accurate model responses. The NARX model was trained for 1000 epochs and its performance was evaluated by changing the number of hidden neurons. It was found that 10 hidden nodes (Figure 3) provided the most effective network architecture similar to the observations of (Jazayeri, Jazayeri, and Uysal 2016; Mohanty, Patra, and Sahoo 2016).

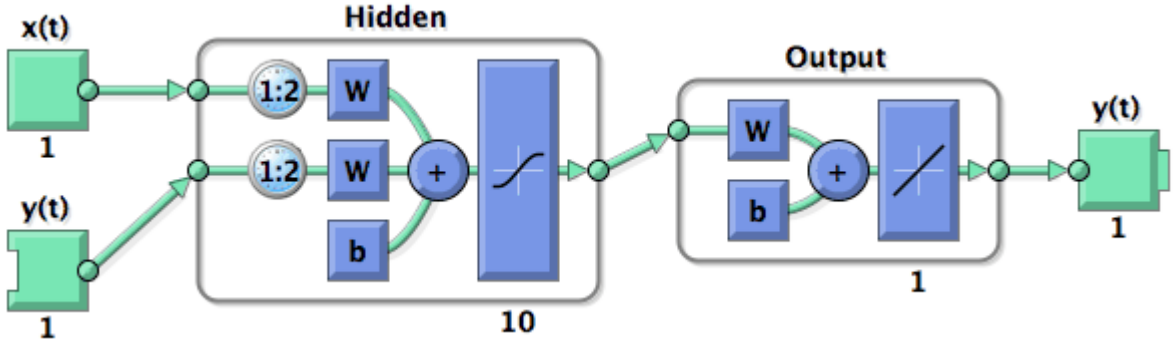

Fig. 3 Series-parallel NARX network

For all the algorithms, the minimum gradient was set to 1.0e−10 as the training goal to achieve accuracy and generalization capabilities at the same time. Seventy percent of the normalized data was used for training, 15% for validation to tune the hyperparameters of the model, and 15% for testing the performance of the models.

The normalized values of the solar parameters were fed to the network through the input layer as shown in Fig. 4. The inputs passed through the hidden layer comprising 10 hidden neurons having a tan-sigmoid transfer function, and reached the output layer comprising one neuron with a linear transfer function. The estimated output was compared with the target output, and the error was back-propagated through the network. After 1000 epochs of backpropagations and weight adjustments, the training goal was achieved and the network generalized new outputs was produced.

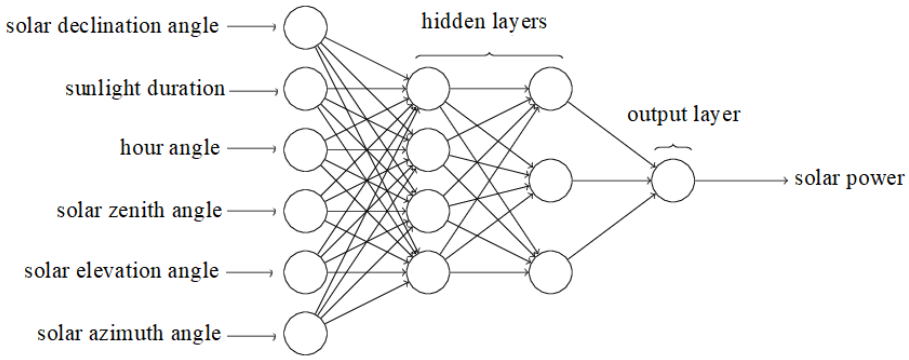

Fig. 4 NARX model architecture

The accuracy of the models was tested by evaluating the RMSE, R^2, U, and SDR between the predicted and actual values of solar power using Eqs. (25)–(29) according to (Madugu et al. 2019; Fentis et al. 2017; Khalil and Shaffie 2013; Banadkooki et al. 2019). The lowest values of RMSE and U provide the best performance. Besides, R^2 and SDR lie between 0 and 1, of which values closest to unity provide the best performance.

$$RMSE = \sqrt{\frac{1}{n}\sum_{n-1}^{n}(E_p - E_a)^2} \tag{25}$$

$$R^2 = \frac{\sum(E_p - E_a)^2}{\sum E_p{}^2 - \frac{\sum E_a{}^2}{n}} \tag{26}$$

$$U = \frac{\left[\sum_{t=1}^{n}\left(\frac{(E_p - E_a)^2}{n}\right)\right]^{1/2}}{\left[\sum_{t-1}^{n}\frac{E_p{}^2}{n}\right]^{1/2} \times \left[\sum_{t-1}^{n}\frac{E_a{}^2}{n}\right]^{1/2}} \tag{27}$$

$$SDR = sd(E_a) - \sum\frac{|E_p|}{|E_a|}sd(E_p) \tag{28}$$

where E_p and E_a are the predicted and actual values of the solar power, respectively, and n is the number of observations.

RESULTS AND DISCUSSIONS

The comparison of the predicted solar power by the four NARX algorithms (BFGS, BR, LM, and SCG) with the actual data for training and testing in the 20 stations spread over four climatic regions are shown in Table 1. It can be observed from the table that the actual values are closely related to the values predicted by the NARX models with minimum residues. Furthermore, the NARX-BR model had the lowest residue of -3.515 W/m^2 in Minna in the Guinea Savanna zone and -2.837 W/m^2 in Akure in the Coastal zone. Similarly, NARX-LM model had the lowest residue of -4.119 W/m^2 in Kano in the Sahel zone, whereas NARX-SCG model had the lowest residue of -4.037 W/m^2 in Iseyin in the Sahel zone.

Tables 2–4 present the performance evaluation of the NARX models over the 20 stations in Nigeria. There was a strong correlation between the predicted and actual values of the solar power for all the models, with the R^2 value exceeding 70% in all the stations. This confirms the suitability and validity of the four NARX algorithms for the prediction of solar power over the stations. Generally, the lower the values of the RMSE metrics, the better the performance of the ANN model. The NARX-BFGS model had the lowest RMSE values of 0.418 W/m^2 in Maiduguri in the Sahel zone, 0.162 W/m^2 in Abuja in the Guinea

Savanna zone, 0.237 W/m^2 in Ibadan in the Derived Savanna zone, and 0.226 W/m^2 in Enugu the Coastal zone. For the NARX-BR model, the lowest RMSE values were 0.404 W/m^2 in Maiduguri in the Sahel zone, 0.181 W/m^2 in Abuja in the Guinea Savanna zone, 0.298 W/m^2 in Ibadan and Ado-Ekiti in the Derived Savanna zone, and 0.213 W/m^2 in Akure in the Coastal zone. Meanwhile, the lowest RMSE for the NARX-LM model were 0.394 0.418 W/m^2 in Maiduguri in the Sahel zone, 0.174 W/m^2 in Abuja in the Guinea Savanna zone, 0.221 W/m^2 in Makurdi in the Derived Savanna zone, and 0.213 W/m^2 in Akure in the Coastal zone. In addition, the lowest RMSE for the NARX-SCG model were 0.394 W/m^2 in Maiduguri in the Sahel zone, 0.181 W/m^2 in Abuja in the Guinea Savanna zone, 0.204 W/m^2 in Makurdi in the Derived Savanna zone, and 0.221 W/m^2 in Enugu the Coastal zone. Furthermore, all the models had U values below 0.7. For instance, the NARX-BFGS model had the lowest U values of 0.438 in Maiduguri in the Sahel zone, 0.179 in Abuja in the Guinea Savanna zone, 0.289 in Ibadan in the Derived Savanna zone, and 0.285 in Port Harcourt Ibadan in the Coastal zone. Additionally, all the models had high SDR values above 0.7.

Table 1 Comparison of the actual and predicted mean solar power by the NARX algorithms over 20 selected stations in four climatic regions of Nigeria

Zone	Station	Mean solar power (W/m^2)					Mean error			
		Actual	BFGS	BR	LM	SCG	BFGS	BR	LM	SCG
Sahel	Sokoto	70.580	70.535	71.878	71.294	70.567	0.045	-1.298	-0.714	0.013
	Gusau	67.221	68.445	67.655	67.658	69.146	-1.224	-0.434	-0.437	-1.925
	Kano	65.007	65.563	65.048	69.126	66.220	-0.556	-0.041	-4.119	-1.213
	Katsina	70.869	65.884	71.211	70.210	70.551	4.985	-0.341	0.660	0.319
	Maiduguri	62.948	63.173	62.847	63.462	62.831	-0.224	0.101	-0.514	0.117
Guinea	Kontagora	43.665	44.858	45.971	44.561	44.514	-1.193	-2.306	-0.896	-0.849
	Minna	41.533	41.645	45.047	41.913	42.052	-0.112	-3.515	-0.380	-0.520
	Abuja	2.151	2.162	2.163	2.163	2.167	-0.011	-0.012	-0.012	-0.017
	Jos	67.090	65.840	66.829	65.712	66.260	1.250	0.261	1.377	0.830
	Yola	49.667	51.498	49.912	50.536	53.140	-1.831	-0.246	-0.869	-3.473
Derived	Ilorin	33.114	34.582	33.547	34.071	34.657	-1.468	-0.433	-0.958	-1.543
	Iseyin	33.150	34.299	34.951	35.424	37.187	-1.149	-1.801	-2.273	-4.037
	Ibadan	26.665	27.885	27.142	27.709	27.940	-1.219	-0.477	-1.043	-1.275
	Ado-Ekiti	27.089	28.084	28.281	30.037	28.136	-0.995	-1.192	-2.948	-1.047
	Makurdi	27.924	28.667	28.110	28.376	28.859	-0.743	-0.186	-0.451	-0.934
Coastal	Ikeja	33.675	36.114	34.810	34.898	35.071	-2.439	-1.136	-1.223	-1.397
	Akure	23.692	25.965	26.530	26.220	24.213	-2.273	-2.837	-2.528	-0.521
	Benin	24.955	26.689	25.960	26.415	26.377	-1.733	-1.004	-1.459	-1.421
	Enugu	25.806	25.894	25.968	26.580	25.856	-0.088	-0.161	-0.774	-0.050
	PH	26.848	25.021	28.423	27.234	29.082	1.827	-1.575	-0.386	-2.234

Table 2 Performance evaluation of NARX-BFGS model

Zone	Station	Train				Test			
		R^2	RMSE	U	SDR	R^2	RMSE	U	SDR
Sahel	Sokoto	0.772	0.466	0.478	0.887	0.776	0.491	0.473	0.896
	Gusau	0.821	0.413	0.423	0.906	0.808	0.419	0.439	0.925
	Kano	0.767	0.475	0.484	0.895	0.744	0.462	0.498	0.886
	Katsina	0.730	0.514	0.521	0.902	0.657	0.544	0.601	0.816
	Maiduguri	0.784	0.471	0.464	0.884	0.802	0.418	0.438	0.946
Guinea	Kontagora	0.853	0.384	0.384	0.901	0.869	0.311	0.341	0.878
	Minna	0.809	0.494	0.490	0.965	0.760	0.435	0.594	1.182
	Abuja	0.962	0.195	0.196	0.967	0.959	0.162	0.179	0.977
	Jos	0.827	0.417	0.415	0.905	0.749	0.379	0.499	0.898
	Yola	0.827	0.419	0.416	0.917	0.786	0.315	0.429	0.918
Derived	Ilorin	0.852	0.406	0.384	0.929	0.785	0.314	0.417	0.927

	Iseyin	0.873	0.371	0.356	0.921	0.838	0.269	0.351	0.808
	Ibadan	0.889	0.356	0.332	0.935	0.879	0.237	0.289	0.962
	Ado-Ekiti	0.887	0.353	0.335	0.915	0.884	0.284	0.339	0.833
	Makurdi	0.883	0.340	0.342	0.943	0.778	0.258	0.387	0.848
Coastal	Ikeja	0.908	0.330	0.304	0.929	0.871	0.299	0.361	0.898
	Akure	0.882	0.363	0.340	0.939	0.890	0.238	0.287	1.023
	Benin	0.903	0.329	0.310	0.931	0.908	0.237	0.287	0.923
	Enugu	0.883	0.349	0.341	0.938	0.873	0.226	0.319	0.921
	PH	0.889	0.329	0.333	0.926	0.918	0.318	0.285	0.904

Table 3 Performance evaluation of NARX-BR model

Zone	Station	Train				Test			
		R^2	RMSE	U	SDR	R^2	RMSE	U	SDR
Sahel	Sokoto	0.761	0.480	0.492	0.834	0.754	0.515	0.496	0.844
	Gusau	0.817	0.417	0.427	0.911	0.807	0.420	0.440	0.934
	Kano	0.757	0.485	0.494	0.858	0.730	0.475	0.512	0.857
	Katsina	0.722	0.521	0.528	0.890	0.736	0.465	0.513	0.862
	Maiduguri	0.772	0.484	0.478	0.878	0.812	0.404	0.423	0.921
Guinea	Kontagora	0.842	0.397	0.397	0.909	0.864	0.317	0.347	0.963
	Minna	0.755	0.550	0.545	0.761	0.650	0.453	0.618	0.779
	Abuja	0.962	0.195	0.196	0.970	0.949	0.181	0.200	0.974
	Jos	0.812	0.434	0.433	0.917	0.709	0.411	0.540	0.907
	Yola	0.838	0.392	0.402	0.915	0.903	0.325	0.306	0.952
Derived	Ilorin	0.880	0.366	0.346	0.911	0.879	0.245	0.326	0.861
	Iseyin	0.865	0.383	0.367	0.921	0.805	0.295	0.385	0.828
	Ibadan	0.874	0.379	0.353	0.942	0.874	0.245	0.298	0.943
	Ado-Ekiti	0.889	0.349	0.331	0.926	0.893	0.249	0.298	0.868
	Makurdi	0.888	0.332	0.334	0.940	0.832	0.224	0.337	0.885
Coastal	Ikeja	0.890	0.364	0.336	0.921	0.839	0.343	0.414	0.872
	Akure	0.890	0.352	0.329	0.937	0.910	0.213	0.257	0.987
	Benin	0.883	0.361	0.340	0.945	0.909	0.236	0.286	1.038
	Enugu	0.876	0.364	0.355	0.928	0.877	0.225	0.317	0.938
	PH	0.888	0.331	0.336	0.924	0.918	0.332	0.298	0.855

Table 4 Performance evaluation of NARX-LM model

Zone	Station	Train				Test			
		R^2	RMSE	U	SDR	R^2	RMSE	U	SDR
Sahel	Sokoto	0.761	0.477	0.489	0.879	0.731	0.539	0.520	0.877
	Gusau	0.839	0.392	0.401	0.895	0.817	0.409	0.428	0.938
	Kano	0.773	0.468	0.476	0.887	0.776	0.434	0.469	0.920
	Katsina	0.711	0.534	0.541	0.903	0.730	0.472	0.522	0.900
	Maiduguri	0.775	0.481	0.474	0.887	0.822	0.394	0.413	0.945
Guinea	Kontagora	0.845	0.394	0.394	0.924	0.847	0.336	0.368	0.992
	Minna	0.845	0.397	0.394	0.910	0.823	0.286	0.390	0.937
	Abuja	0.961	0.195	0.196	0.974	0.954	0.174	0.192	0.964
	Jos	0.806	0.442	0.440	0.920	0.701	0.418	0.550	0.904
	Yola	0.840	0.389	0.399	0.910	0.883	0.358	0.338	0.935
Derived	Ilorin	0.851	0.408	0.386	0.903	0.790	0.313	0.415	0.916
	Iseyin	0.872	0.373	0.357	0.922	0.606	0.448	0.586	0.720
	Ibadan	0.806	0.442	0.440	0.920	0.701	0.418	0.550	0.904
	Ado-Ekiti	0.889	0.350	0.332	0.913	0.887	0.266	0.317	0.841
	Makurdi	0.887	0.336	0.338	0.957	0.837	0.221	0.332	0.909
Coastal	Ikeja	0.900	0.343	0.316	0.925	0.877	0.293	0.354	0.894
	Akure	0.887	0.356	0.333	0.934	0.879	0.247	0.297	0.906

	Benin	0.898	0.337	0.318	0.932	0.913	0.222	0.270	0.937
	Enugu	0.935	0.276	0.269	0.878	0.934	0.183	0.259	0.846
	PH	0.885	0.335	0.340	0.926	0.898	0.355	0.319	0.885

Table 5 Performance evaluation of NARX-SCG model

Zone	Station	Train				Test			
		R^2	RMSE	U	SDR	R^2	RMSE	U	SDR
Sahel	Sokoto	0.783	0.456	0.467	0.872	0.790	0.476	0.459	0.869
	Gusau	0.805	0.431	0.442	0.919	0.807	0.422	0.442	0.942
	Kano	0.762	0.479	0.488	0.888	0.739	0.472	0.510	0.918
	Katsina	0.715	0.530	0.537	0.899	0.714	0.486	0.537	0.884
	Maiduguri	0.781	0.474	0.468	0.885	0.821	0.394	0.413	0.916
Guinea	Kontagora	0.854	0.382	0.382	0.918	0.854	0.326	0.358	0.958
	Minna	0.837	0.407	0.403	0.915	0.766	0.331	0.452	0.941
	Abuja	0.961	0.197	0.198	0.969	0.953	0.174	0.192	0.966
	Jos	0.823	0.421	0.420	0.911	0.738	0.387	0.509	0.886
	Yola	0.846	0.383	0.392	0.905	0.893	0.341	0.321	0.935
Derived	Ilorin	0.884	0.362	0.342	0.900	0.843	0.279	0.371	0.856
	Iseyin	0.869	0.376	0.361	0.924	0.704	0.374	0.489	0.879
	Ibadan	0.889	0.356	0.331	0.936	0.873	0.250	0.303	0.897
	Ado-Ekiti	0.892	0.351	0.332	0.895	0.900	0.278	0.332	0.799
	Makurdi	0.892	0.326	0.328	0.934	0.865	0.204	0.307	0.862
Coastal	Ikeja	0.895	0.351	0.324	0.936	0.875	0.301	0.364	0.898
	Akure	0.889	0.353	0.330	0.937	0.895	0.223	0.269	0.971
	Benin	0.900	0.333	0.314	0.934	0.891	0.250	0.304	0.981
	Enugu	0.884	0.348	0.340	0.932	0.881	0.221	0.311	0.925
	PH	0.846	0.383	0.392	0.905	0.893	0.341	0.321	0.935

Figures 5 and 6 show the comparison of the algorithms based on R^2 and RMSE, respectively. The Coastal zone had the highest R^2 values for all the algorithms, except NARX-SCG algorithm for which the highest R^2 value occurred in the Derived Savanna zone. Furthermore, whereas the Derived Savanna zone the lowest R^2 values. Furthermore, the highest RMSE values occurred in the Sahel zone for all the algorithms, whereas the lowest RMSE values occurred in the Derived Savanna zone. The NARX-BFGS algorithm had the best performance among the other algorithms for the Coastal and Guinea Savanna zones owing to their lowest RMSE and highest R^2 values. Similarly, the NARX-LM and NARX-BR algorithms had the best performance in the Sahel and Derived Savanna zones, respectively.

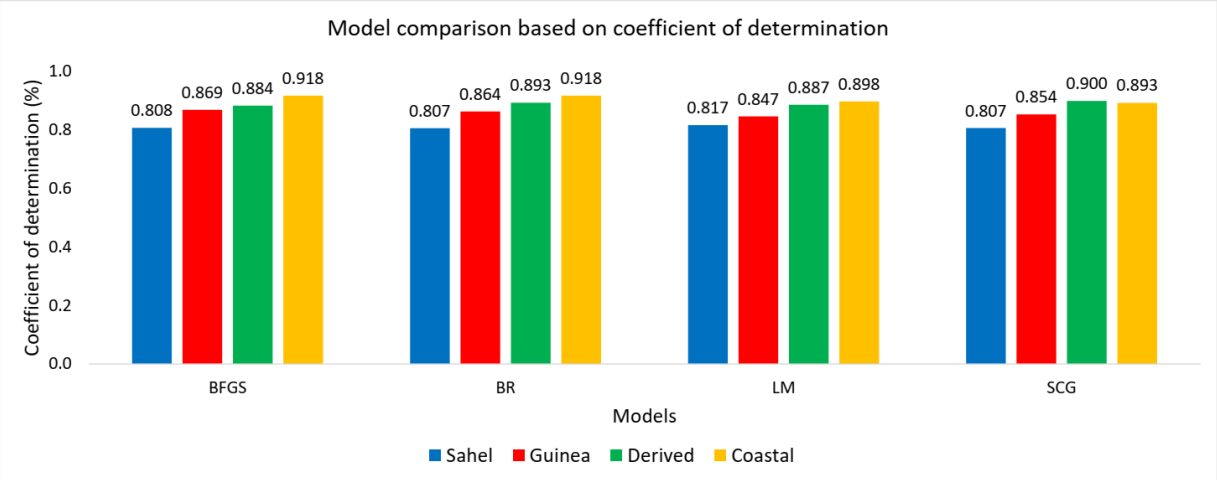

Fig. 5 Comparison of models based on coefficient of determination

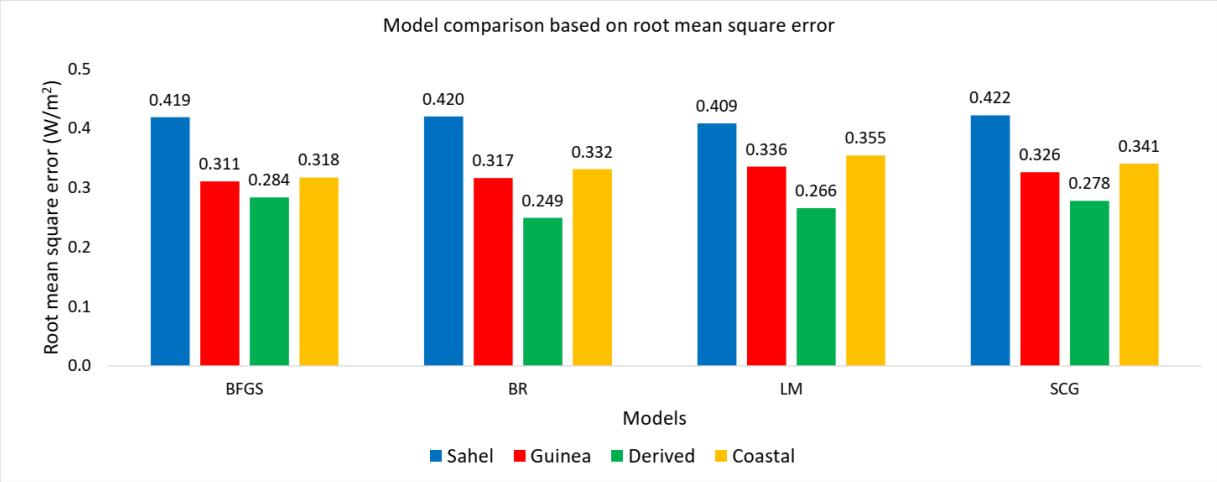

Fig. 6 Comparison of models based on root mean square error

CONCLUSION

In this study, the surface data of direct and diffuse solar radiation were obtained from the archives of MERRA-2 for 20 stations spread across Nigeria. Four NARX models were employed to estimate the solar power for the different geoclimatic zones of Nigeria, and the most appropriate algorithm for each geoclimatic zone was identified. The assessment of the models using statistical metrics showed that all the models had desirable performance with RMSE values ranging from 0.162 to 0.544 W/m^2. Furthermore, all the values predicted by the models had strong correlations with the actual values, with R^2 exceeding 70%. On a regional basis, NARX-BFGS algorithm had the best performance in the Coastal and Guinea Savanna zones, whereas NARX-LM and NARX-BR algorithms had the best performances in the Sahel and Derived Savanna zones, respectively. The proposed models can be used to predict the solar power in any location within each of the four geoclimatic regions of Nigeria. Moreover, other machine learnings techniques can be explored to estimate solar power in Nigeria in comparison with the NARX model used in this study.

REFERENCES

Abuella M, Chowdhury B (2015) Solar Power Forecasting Using Artificial Neural Networks. 2015 North American Power Symposium, NAPS 2015, no. October. https://doi.org/10.1109/NAPS.2015.7335176.

Asirvadam VS, McLoone SF, Irwin GW (2004) Memory Efficient BFGS Neural-Network Learning Algorithms Using MLP-Network: A Survey. Proceedings of the 2004 IEEE International Conference on Control Applications, 1:586-591 Vol. 1.

https://doi.org/10.1109/CCA.2004.1387275.

Awan SM, Khan ZA, Aslam M (2018) Solar Generation Forecasting by Recurrent Neural Networks Optimized by Levenberg-Marquardt Algorithm. IECON 2018 - 44th Annual Conference of the IEEE Industrial Electronics Society, 276–81. https://doi.org/10.1109/IECON.2018.8591799.

Banadkooki FB, Mohammad E, Ali NA, Chow MF, Haitham AA et al (2019) Precipitation Forecasting Using Multilayer Neural Network and Support Vector Machine Optimization Based on Flow Regime Algorithm Taking into Account Uncertainties of Soft Computing Models. Sustainability 11 (23). https://doi.org/10.3390/su11236681.

Bishop CM (1995) Deep Neural Networks for Pattern Recognition. Clarendon Press, London.

Bugaje IM (2006) Renewable Energy for Sustainable Development in Africa: A Review. Renewable and Sustainable Energy Reviews 10 (6): 603–12. https://doi.org/10.1016/j.rser.2004.11.002.

Çoruh S, Feza G, Erdal K, Ufuk Ç (2014) The Use of NARX Neural Network for Modeling of Adsorption of Zinc Ions Using Activated Almond Shell as a Potential Biosorbent. Bioresource Technology 151: 406–10. https://doi.org/10.1016/j.biortech.2013.10.019.

Diaconescu E (2008) The Use of NARX Neural Networks to Predict Chaotic Time Series. WSEAS Transactions on Computer Research 3(3): 182–91.

El-Sebaii AA, Al-Hazmi FS, Al-Ghamdi AA, Yaghmour SJ (2010) Global, Direct and Diffuse Solar Radiation on Horizontal and Tilted Surfaces in Jeddah, Saudi Arabia. Applied Energy 87(2): 568–76. https://doi.org/10.1016/j.apenergy.2009.06.032.

Fentis A, Bahatti L, Mestari M, Chouri B (2017) Short-Term Solar Power Forecasting Using Support Vector Regression and Feed-Forward NN. 2017 15th IEEE International New Circuits and Systems Conference (NEWCAS), 405–8. https://doi.org/10.1109/NEWCAS.2017.8010191.

Guzman SM, Joel OP, Mary LMT (2017) The Use of NARX Neural Networks to Forecast Daily Groundwater Levels. Water Resources Management 31 (5): 1591–1603. https://doi.org/10.1007/s11269-017-1598-5.

Haddad S, Benghanem M, Mellit A, Daffallah KO (2015) ANNs-Based Modeling and Prediction of Hourly Flow Rate of a Photovoltaic Water Pumping System: Experimental Validation. Renewable and Sustainable Energy Reviews 43: 635–43. https://doi.org/10.1016/j.rser.2014.11.083.

Inman RH, Hugo TCP, Carlos FMC (2013) Solar Forecasting Methods for Renewable Energy Integration. Progress in Energy and Combustion Science 39 (6): 535–76. https://doi.org/https://doi.org/10.1016/j.pecs.2013.06.002.

Iqbal M (1983). An Introduction to Solar Radiation. Academic Press, Canada.

Jazayeri K, Moein J, Sener U (2016) Comparative Analysis of Levenberg-Marquardt and Bayesian Regularization Backpropagation Algorithms in Photovoltaic Power Estimation Using Artificial Neural Network. Lecture Notes in Computer Science (Including Subseries Lecture Notes in Artificial Intelligence and Lecture Notes in Bioinformatics) 9728: 80–95. https://doi.org/10.1007/978-3-319-41561-1_7.

Katiyar AK, Panday CK (2010) Study of Ground-Reflected Component and Its Contribution in Diffuse Solar Radiation Incident on Inclined Surfaces over India. International Journal of Energy and Environment 1(3): 547–54. https://doi.org/10.1016/j.desal.2007.01.030.

Khalil SA, Shaffie AM (2013) A Comparative Study of Total, Direct and Diffuse Solar Irradiance by Using Different Models on Horizontal and Inclined Surfaces for Cairo, Egypt. Renewable and Sustainable Energy Reviews 27: 853–63. https://doi.org/10.1016/j.rser.2013.06.038.

Kumar P, Merchant SN, Desai UB (2004) Improving Performance in Pulse Radar Detection Using Bayesian Regularization for Neural Network Training. Digital Signal Processing: A Review Journal 14 (5): 438–48. https://doi.org/10.1016/j.dsp.2004.06.002.

Madugu IS, Olufeagba BJ, Yinusa AA, Abdulkadir F et al (2019) A Novel Model for Solar Radiation Prediction. Telkomnika (Telecommunication Computing Electronics and Control) 17(6): 3100–3109. https://doi.org/10.12928/TELKOMNIKA.v17i6.12729.

Maind SB, Priyanka W (2014) Research Paper on Basic of Artificial Neural Network. International Journal on Recent and Innovation Trends in Computing and Communication 2 (1): 96–100.

Markos FM, Sentian J (2016) Potential of Solar Energy in Kota Kinabalu , Sabah : An Estimate Using a Photovoltaic System Model Potential of Solar Energy in Kota Kinabalu , Sabah : An Estimate Using a Photovoltaic System Model. Journal of Physics: Conference Series, 710. https://doi.org/10.1088/1742-

6596/710/1/012032.

Mishra S, Rajashree P, Pradosh KH (2016) Analysis of Levenberg-Marquardt and Scaled Conjugate Gradient Training Algorithms for Artificial Neural Network Based LS and MMSE Estimated Channel Equalizers. Proceedings - 2015 International Conference on Man and Machine Interfacing, MAMI 2015, no. Lm. https://doi.org/10.1109/MAMI.2015.7456617.

Mohanty S, Prashanta KP, Sudhansu SS (2016) Prediction of Global Solar Radiation Using Nonlinear Auto Regressive Network with Exogenous Inputs (Narx). Proceedings of the 2015 39th National Systems Conference, NSC 2015. https://doi.org/10.1109/NATSYS.2015.7489103.

Mukherjee I, Srikanta R (2012) Comparing the Performance of Neural Networks Developed by Using Levenberg–Marquardt and Quasi-Newton with the Gradient Descent Algorithm for Modelling a Multiple Response Grinding Process. Expert Systems with Applications 39(3): 2397–2407. https://doi.org/https://doi.org/10.1016/j.eswa.2011.08.087.

Ojo OS, Adeyemi B (2020) Application of Nonlinear Autoregressive Neural Network to Estimation of Global Solar Radiation over Nigeria. Journal of Advances in Science and Engineering (JASE) 3.

Ojo OS, Adeyemi B, Oluleye DO (2020) Artificial Neural Network Models for Prediction of Net Radiation over a Tropical Region. Neural Computing and Applications 9. https://doi.org/10.1007/s00521-020-05463-9.

Olusola OS, Emmanuel I, Oluwafemi O, Adeyemi B (2020) Determination of Optimal Solar Power and Corresponding Tilt Angles in Different Geoclimatic Zones in Nigeria. Journal of Energy Research and Reviews.

Ozoegwu CG (2019) Artificial Neural Network Forecast of Monthly Mean Daily Global Solar Radiation of Selected Locations Based on Time Series and Month Number. Journal of Cleaner Production 216: 1–13. https://doi.org/https://doi.org/10.1016/j.jclepro.2019.01.096.

Pandey CK, Katiyar AK (2009) A Note on Diffuse Solar Radiation on a Tilted Surface. Energy 34 (11): 1764–69. https://doi.org/10.1016/j.energy.2009.07.006.

Rajendra P, Murthy KVN, Subbarao A, Rahul B (2019) Use of ANN Models in the Prediction of Meteorological Data. Modeling Earth Systems and Environment 5 (3): 1051–58. https://doi.org/10.1007/s40808-019-00590-2.

Sani MG, Norhaliza AW, Yahya MS, Sharatul IS, Irma WJ (2014) Comparison of NARX Neural Network and Classical Modelling Approaches. Mechanical and Materials Engineering, 554:360–65. Applied Mechanics and Materials. Trans Tech Publications Ltd. https://doi.org/10.4028/www.scientific.net/AMM.554.360.

Sözen A, Erol A, Mehmet Ö, Naci Ç (2005) Forecasting Based on Neural Network Approach of Solar Potential in Turkey. Renewable Energy 30 (7): 1075–90. https://doi.org/10.1016/j.renene.2004.09.020.

Tikyaa EV, Matthias IE, Bernadette CI, Alexander NA (2018) A Hybrid SARIMA-NARX Nonlinear Dynamics Model for Predicting Solar Radiation in Makurdi. International Journal of Mathematics and Computational Science 4 (2): 35–47.

Verma T, Tiwana APS, Reddy CC, Arora V, Devanand P (2016) Data Analysis to Generate Models Based on Neural Network and Regression for Solar Power Generation Forecasting. 2016 7th International Conference on Intelligent Systems, Modelling and Simulation (ISMS), 97–100. https://doi.org/10.1109/ISMS.2016.65.

Zhang N, Pradeep KB (2012) Solar Radiation Prediction Based on Recurrent Neural Networks Trained by Levenberg-Marquardt Backpropagation Learning Algorithm. 2012 IEEE PES Innovative Smart Grid Technologies, ISGT 2012. https://doi.org/10.1109/ISGT.2012.6175757.